Hidden scale invariance at high pressures in gold and five other face-centered-cubic metal crystals

Laura Friedeheim,* Jeppe C. Dyre, and Nicholas P. Bailey
"Glass and Time," IMFUFA, Department of Science and Environment, Roskilde University, P.O. Box 260, DK-4000 Roskilde, Denmark

(Received 18 October 2018; published 27 February 2019)

Recent density functional theory simulations showed that metals have a hitherto overlooked symmetry termed "hidden scale invariance" [Hummel *et al.*, Phys. Rev. B **92**, 174116 (2015)]. This scaling property implies the existence of lines in the thermodynamic phase diagram, so-called isomorphs, along which structure and dynamics are invariant to a good approximation when given in properly reduced units. This means that the phase diagram becomes effectively one-dimensional with regard to several physical properties. This paper investigates consequences and implications of the isomorph theory in six metallic crystals: Au, Ni, Cu, Pd, Ag, and Pt. The data are obtained from molecular dynamics simulations employing many-body effective medium theory (EMT) to model the atomic interactions realistically. We test the predictions from isomorph theory for structure and dynamics by means of the radial distribution and the velocity autocorrelation functions, as well as the prediction of instantaneous equilibration after a jump between two isomorphic state points. Many properties of crystals tend to be dominated by defects, and many of the properties associated with these defects are expected to be isomorph invariant as well. This is investigated in this paper for the case of vacancy diffusion. In regard to the perfect crystal properties, we find the predicted invariance of structure and also, though less perfectly, of dynamics. We show results on the variation of the density-scaling exponent γ, which can be related to the Grüneisen parameter, for all six metals. We consider large density changes up to a factor of two, corresponding to very high pressures. Unlike systems modeled using the Lennard-Jones potential where the density-scaling exponent γ is almost constant, this quantity varies substantially when using the EMT potential and is also strongly material dependent.

DOI: 10.1103/PhysRevE.99.022142

I. INTRODUCTION

The most common state of metals as used by humans is the solid (crystal) phase. Investigation of the properties of pure crystalline metals has played a huge role in the development of solid state physics [1], and the mechanical properties of pure metals and alloys have historically been the most important topic in materials science [2]. It might therefore be thought that all of the basic physics of pure crystalline metals have been well understood and documented. However, recent work has demonstrated the existence of a previously unknown approximate scale invariance in a range of model systems, including metals, in both the liquid and crystal phases. Specifically, in the part of the phase diagram corresponding to the condensed phases there exist curves, termed *isomorphs*, along which a large set of physical properties, namely, those relating to structure and microscopic dynamics, as well as some thermodynamic properties and some transport coefficients, are approximately invariant when expressed in appropriately scaled units [3]. Recent *ab initio* simulations [4] have confirmed that many pure metals belong to the class of systems which have good isomorphs, a class known as Roskilde or R-simple systems. It is the purpose of this paper to document isomorph invariance of structure and dynamics of perfect metallic crystals, specifically the fcc metals Au, Ni, Cu, Pd, Ag, and Pt. The work was inspired by a bachelor's degree student project which investigated isomorphs in the liquid state for the same six metals [5].

An early paper [6] presented some evidence that metallic systems belong to the class of R-simple systems. Hu *et al.* have also reported results for a simulated metallic glass [7]. Recently, Hummel *et al.* confirmed using density functional theory (DFT) methods that most metals are R-simple close to their triple point [4]. Because of the large computational cost of DFT methods, other state points were not studied, so the variation of, for example, the density-scaling exponent γ has not been studied. Moreover, the cost of DFT calculations limits what aspects of thermodynamics and structure can be studied and essentially prohibits the study of dynamics and transport coefficients. It is of great interest to investigate and document expected isomorph variances in metallic crystals, liquids, and amorphous structures (metallic glasses) using many-body empirical potentials, which offer a reasonable compromise between computational efficiency and accuracy. In addition, metals form an interesting class of R-simple systems because they are not described by pair interactions (as evidenced by the violation of the Cauchy relations for the elastic constants) [8]; while a good understanding of the density-scaling properties of systems with pair interactions exists [9–11], many-body systems present a challenge: are they R-simple?

In this work we use the effective medium theory (EMT) semiempirical many-body potential [12]. It is considered semiempirical because it is derived from DFT, and some of the parameters are drawn directly from DFT calculations. The expression for the total potential energy is similar in structure

*lauraf@ruc.dk

to other commonly used many-body potentials for metals, such as the embedded atom method (EAM), involving pair sums and some nonlinear "embedding" function. Unlike many EAM potentials, EMT is based on fairly simple functional forms, rather than complex functions which require heavy fitting to large data sets and are typically tabulated. This means that (1) EMT has been relatively straightforward to implement in our graphical processing unit (GPU) molecular dynamics software RUMD [13] and (2) we can hope to understand analytically the existence of strong virial potential-energy correlation in this potential and moreover find an analytic expression for how γ depends on density. We use the simplest version of EMT presented in Ref. [12], which provides all parameters necessary to simulate EMT models of Ni, Cu, Pd, Ag, Pt, and Au.

We restrict our investigation of the isomorph scaling properties of metallic systems to the crystal phases of pure systems, the metal elements listed above. These all have a face-centered-cubic (fcc) ground state at zero pressure. A previous work considered the isomorph scaling properties of classical crystals consisting both of spherical particles interacting via pair potentials, as well as simple molecular systems, and found that simple measures of structure and dynamics are invariant along isomorphs, as expected [14]. We consider the same properties as those authors: we investigate structure as quantified by the radial distribution function (RDF) and dynamics as quantified by the velocity autocorrelation function (VAF), which can be related to the phonon spectrum [15]. Mechanical properties of crystalline materials tend to be dominated by defects, specifically vacancies, interstitials, dislocations, stacking faults, and grain boundaries [16]. Many properties associated with defects are expected to be isomorph invariant—for example, defect mobilities—when expressed in reduced units. As in Ref. [14] we investigate in this work a simple case, namely vacancy diffusion. We also check one of the dramatic predictions of isomorph theory, instantaneous equilibration when a system is brought rapidly from one state point to another on the same isomorph [3].

II. ISOMORPH THEORY AND HIDDEN SCALE INVARIANCE

Isomorph theory has been developed throughout a series of papers [3,6,17–19] starting from first establishing the existence and subsequently developing a theoretical understanding of strong correlations between the equilibrium fluctuations of the configurational parts of pressure and energy. The correlations are deemed strong when $R > 0.9$ where R is the (Pearson) correlation coefficient

$$R = \frac{\langle \Delta W \Delta U \rangle}{\sqrt{\langle (\Delta W)^2 \rangle \langle (\Delta U)^2 \rangle}} \tag{1}$$

with the sharp brackets denoting the canonical constant-volume (NVT) averages, and where W and U are the virial and the potential energy, respectively. Systems with these strong correlations are also referred to as R-simple systems to (1) account for the ambiguity of the term "strongly correlated" in physics and chemistry, (2) stress the fact that these systems exhibit a particularly simple behavior in terms of structure and dynamics, and (3) show that this behavior is not limited to liquids only but extends to the solid phase as well since the strong correlations generally appear when the system is dense [6,17].

Paper IV [3] of the series mentioned above introduced the concept of *isomorphs*. Isomorphs are curves in the phase diagram along which certain static, dynamic, and thermodynamic quantities are invariant when given in appropriately reduced units. Any configuration can be described in terms of the particle coordinates as

$$\boldsymbol{R} = (\boldsymbol{r}_1, \boldsymbol{r}_2, \ldots, \boldsymbol{r}_N) \tag{2}$$

where $\boldsymbol{r}_i$ is the coordinate vector of the ith particle. The reduced unit version is given by $\tilde{\boldsymbol{R}} = \rho^{1/3}\boldsymbol{R}$, where $\rho \equiv N/V$ is the number density. If two configurations from different state points have the same reduced coordinates,

$$\rho_1^{1/3}\boldsymbol{R}_1 = \rho_2^{1/3}\boldsymbol{R}_2, \tag{3}$$

then Roskilde simplicity implies they have approximately proportional configurational NVT Boltzmann factors

$$\exp\left[-\frac{U(\boldsymbol{R}_1)}{k_B T_1}\right] \cong C_{12} \exp\left[-\frac{U(\boldsymbol{R}_2)}{k_B T_2}\right], \tag{4}$$

where the constant C_{12} depends only on the state points (T_1, ρ_1) and (T_2, ρ_2) and not on the configurations. This means that the potential energy of a given configuration $U(\boldsymbol{R}_i)$ at density ρ_i can be scaled to a different density on the same isomorph as follows:

$$U(\boldsymbol{R}_2) \cong \frac{T_2}{T_1} U(\boldsymbol{R}_1) + k_B T_2 C_{12}, \tag{5}$$

or, considering fluctuations about the respective mean values:

$$\Delta U(\boldsymbol{R}_2) \cong \frac{T_2}{T_1} \Delta U(\boldsymbol{R}_1). \tag{6}$$

The shape of an isomorph is characterized in terms of the density-scaling exponent γ defined as the logarithmic derivative of temperature with respect to density along a curve of constant excess entropy. Statistical mechanics provides an expression in terms of fluctuations for this derivative [3], giving

$$\gamma \equiv \left(\frac{\partial \ln T}{\partial \ln \rho}\right)_{S_{\text{ex}}} = \frac{\langle \Delta W \Delta U \rangle}{\langle (\Delta U)^2 \rangle}. \tag{7}$$

"Excess" quantities are defined in reference to the respective quantity for the ideal gas at the same temperature and density, e.g., $S_{\text{ex}} = S - S_{\text{id}}$. Equation (7) allows one to map out isomorphs in a stepwise manner by evaluating γ at each state point. Another way to trace isomorphs is the so-called direct isomorph check (DIC), which exploits the connection between the energies and temperatures of two state points of Eqs. (5) and (6). Hence, plotting the potential energies of the initial microscopic configurations at ρ_1 versus the potential energies of the configurations scaled to another density ρ_2 results in a scatter plot where the slope of the best fit line is given by the ratio of the temperatures, T_2/T_1. An example of such a scatter plot is shown in Fig. 1. The advantage of the direct isomorph check is that this method allows a whole isomorph to be generated from a single simulation at one reference state point. We have checked that the generated temperatures differ by at most 0.5% from isomorphs generated in the stepwise manner by Eq. (7) (see Appendix A).

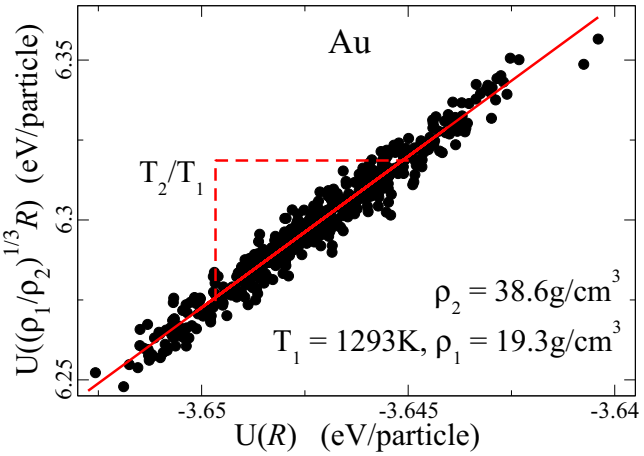

FIG. 1. The direct isomorph check for gold: a scatter plot of potential energies of configurations drawn from a simulation at a given density ρ_1 and temperature T_1 versus the potential energies of the configurations scaled to another density ρ_2. The red line is the best fit line and has the slope T_2/T_1, so the temperature T_2 for a state point with density ρ_2 on the same isomorph as the initial state point can be identified from linear regression. The same initial configuration can be scaled to different densities, thus allowing one to map out several isomorphic points from a single simulation.

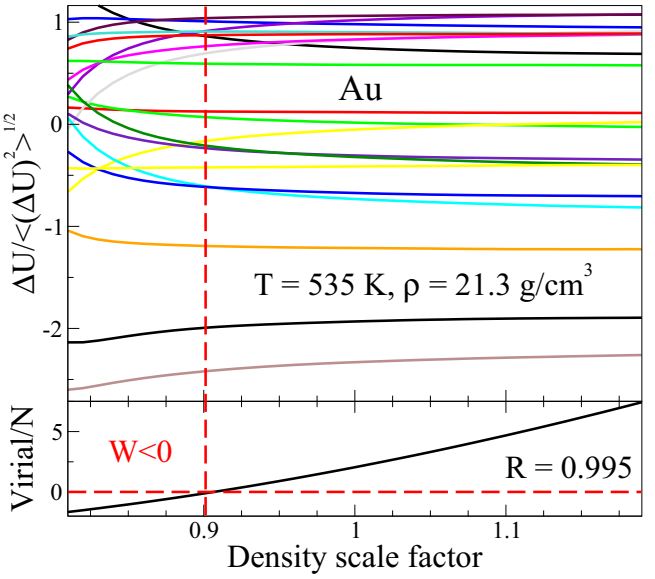

FIG. 2. Gold's potential energy per particle after subtracting the average and scaling by the standard deviation of 20 configurations taken from an equilibrium simulation, which were subsequently scaled uniformly by 20% up and down in density and plotted as a function of the density-scaling factor. The lines obtained in this way illustrate the hidden scale invariance of R-simple systems and cannot cross each other in the ideal ($R = 1$) case. The configurations used for generating this figure are taken from equilibrium simulations at a state point close to ambient conditions at which $R = 0.995$. The bottom panel shows the average virial for the scaled configurations. The strongly diverging lines in the left part of the figure are due to the virial becoming negative (indicated by the red dashed lines).

The existence of isomorphs yields the profound simplification of effectively reducing the (T, ρ)-phase diagram by one dimension. The one-to-one correspondence between state points as illustrated above also explains why many quantities are invariant along isomorphs when given in reduced units. Using the length unit l_0, time unit t_0, and an energy unit e_0 defined as follows:

$$l_0 = \rho^{-1/3}, \quad t_0 = \rho^{-1/3}\sqrt{m/k_BT}, \quad e_0 = k_BT, \qquad (8)$$

all quantities can be expressed in a dimensionless form to compensate for the trivial scaling of lengths by average interparticle spacing and energies by the temperature.

As pointed out in paper IV [3], systems with strong correlations have isomorphs and vice versa, i.e., these two features are equivalent. It was found later that they are both manifestations of an underlying approximate *hidden scale invariance*. Indeed, isomorph theory has been refined in Ref. [20] by defining R-simple systems directly from a scale invariance of the potential-energy function. It is based on the following scaling behavior:

$$U(\boldsymbol{R}_a) < U(\boldsymbol{R}_b) \Rightarrow U(\lambda\boldsymbol{R}_a) < U(\lambda\boldsymbol{R}_b), \qquad (9)$$

where $U(\boldsymbol{R}_i)$ is the potential energy of a configuration $\boldsymbol{R}_i$ and λ is a scaling parameter. Thus, a uniform scaling of configurations does not change the ordering of potential energies. For most systems this scale invariance is approximate and dubbed "hidden" since it is not obvious from the mathematical expression for the potential. This approximate scaling is illustrated in Fig. 2, where the potential energies of 20 configurations from an equilibrium simulation have been scaled to different densities. For clarity the energies have been shifted and scaled using the mean value and standard deviation at each density. For perfectly isomorphic systems—with correlation coefficient $R = 1$—the lines cannot cross each other. The red dashed line indicates where the virial becomes negative, which leads to a breakdown of the scaling properties as seen by the sudden diverging of the lines.

The updated definition preserves the property that isomorphs are the configurational adiabats of the phase diagram, curves along which structure, dynamics, and the excess entropy S_{ex} are invariant together with the simplification of effectively reducing the phase diagram by one dimension. Subtle differences between the versions of isomorph theory emanate from the fact that the original formulation is a first-order approximation of the more accurate updated theory of Ref. [20]. This can be illustrated, for example, using the case of the isochoric heat capacity C_V. If exactly obeyed, Eq. (4) implies that C_V is invariant along isomorphs, which is often a good approximation but not exact. The slight variation of C_V along isomorphs can, however, be accommodated using the more recent formulation of isomorph theory, with which Eq. (6) can be derived without requiring Eq. (4) or (5) [20].

One of the more fundamental consequences of the update concerns the density-scaling exponent γ. Initially the density-scaling exponent γ was interpreted as being related to an effective inverse power law exponent, which (assuming it to be constant) yields the form $\rho^\gamma/T = \text{const}$ for isomorphs, consistent with experimental determinations of isochrones [10,21–26]. Determination of γ from fluctuations in simulations shows variation with state point, however [6]. It was

TABLE I. Comparison of correlation coefficient R and density-scaling exponent γ calculated using DFT and using EMT. A liquid state point near the triple point is used in each case. The DFT values are taken from Ref. [4].

Sym.	Z	T (K)	$\rho\left(\frac{g}{cm^3}\right)$	R_{EMT}	R_{DFT}	γ_{EMT}	γ_{DFT}
Ni	28	2000	8.19	0.96	0.92(0.03)	3.62(0.01)	3.5(0.3)
Cu	29	1480	8.02	0.95	0.90(0.02)	4.15(0.02)	4.1(0.2)
Pd	46	1900	10.38	0.91	0.92(0.04)	6.47(0.03)	4.9(0.5)
Ag	47	1350	9.32	0.93	0.90(0.03)	5.35(0.02)	4.8(0.4)
Pt	78	2200	18.53	0.87	0.87(0.06)	7.88(0.05)	6.0(1.4)
Au	79	1470	16.69	0.88	0.86(0.14)	7.93(0.05)	7.9(1.6)

shown in Ref. [11] that the assumption of constant C_V along isomorphs implies that γ can depend only on density, which is a fairly good approximation. The most recent definition of hidden scale invariance allows, however, temperature dependence of γ also to be handled within the theory [20].

We find, in fact, that for metals—at least when using the EMT potential—γ does vary significantly, both for a given metal and between metals. Table I shows a comparison of the DFT and EMT values of the parameters R and γ for the liquid phase near the triple point. There is reasonable agreement between the R and γ values, especially noting that the latter vary quite widely (more than a factor of two). From this we can conclude that EMT gives a reasonably accurate description of the thermodynamic scaling properties of these metals. A version of this table appeared in Ref. [5].

III. SIMULATION RESULTS

The results presented in this paper for the fcc metals Ni, Cu, Pd, Ag, Pt, and Au have been obtained from simulations carried out in RUMD [13,27] using the effective medium theory (EMT) potential. The potential is based on a reference system modified with a correction term. The reference system is chosen to give a close to accurate description while still being a simple, well-known system which can be fitted through some built-in scaling parameter. For metal crystals this can be achieved with an ideal fcc lattice where the lattice constant serves as the scaling parameter. The correction term accounts for the difference between the real and the reference system and is based on a pair potential. A detailed description of the potential and the respective material-specific parameters is given in Ref. [12].

The simulated systems consist of 4000 particles organized on a $10 \times 10 \times 10$ fcc lattice with periodic boundary conditions. Atomic masses and densities are taken from Ref. [28].

For each metal, we simulate at least three curves: one isomorph, one isotherm, and one isochore. The state points for the isomorph have been determined using a single simulation and the direct isomorph check, as described in the previous section. We obtain isomorphic points corresponding to steps of 10% density change in terms of the reference density up to a total increase of 100% in density. The state points for the isochore (isotherm) are chosen so that they match the temperatures (densities) of the points along the isomorph. The initial state point for each metal is chosen to resemble a crystal with room temperature density, $\rho_{r.t.}$ ([28]), at 1293 K for gold, corresponding to a pressure of 10 GPa. The isotherm is along $T = 1293.15$ K and thus shares the initial point with the isomorph. To avoid melting on isochores, they start at higher densities, $\rho = 32.84$ g/cm^3 for the investigation of structural and dynamical invariance and $\rho = 30.91$ g/cm^3 for the vacancy study.

TABLE II. Pressure P, virial W, correlation coefficient R, and density-scaling exponent γ along the studied isomorph for gold.

T (K)	$\rho\left(\frac{g}{cm^3}\right)$	P (GPa)	$W\left(\frac{eV}{\text{particle}}\right)$	R	γ
1293	19.32	10	0.86	0.986	6.47
2177	21.25	30	3.03	0.994	4.66
3143	23.18	70	5.58	0.996	3.77
4175	25.12	110	8.50	0.997	3.25
5255	27.05	160	11.73	0.998	2.90
6374	28.98	220	15.25	0.998	2.63
7522	30.91	300	19.03	0.998	2.44
8692	32.84	380	23.05	0.998	2.27
9879	34.78	480	27.29	0.998	2.14
11 073	36.71	590	31.71	0.998	2.02
12 270	38.64	710	36.32	0.998	1.92

For each state point the NVT ensemble was simulated using periodic boundary conditions and a Nosé-Hoover thermostat. Table II shows the temperatures and densities for the isomorph simulated for Au, while Fig. 3 shows the isomorph together with the melting curve for this system. The latter was determined using the interface pinning method [29]. A single point from the experimental melting curve is included, showing that it lies somewhat higher in temperature than the model curve. A slight discrepancy between model and experiment is expected if the model has not explicitly been fitted to the melting temperature. Melting is identified as the point where the Gibbs free energies of the solid and the liquid phase are equal, thus a precise prediction for the melting

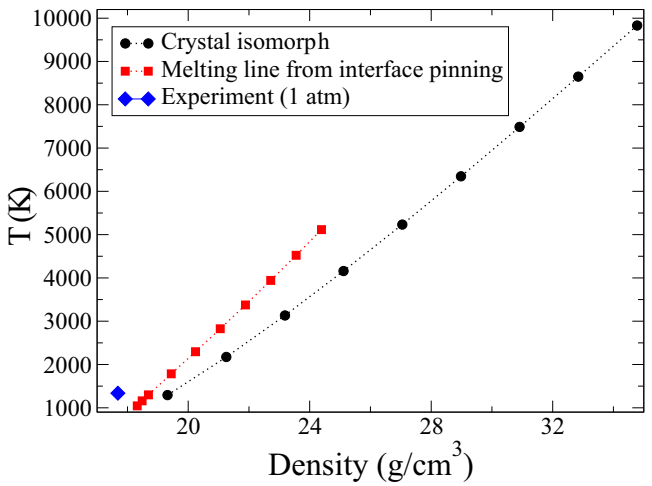

FIG. 3. A density-temperature phase diagram of EMT-Au showing the melting curve determined by the interface-pinning method [29] and the crystal isomorph studied in this work. One point from the experimental melting curve is also included [30]. The isomorph for Au studied in this work is quite close to the melting curve.

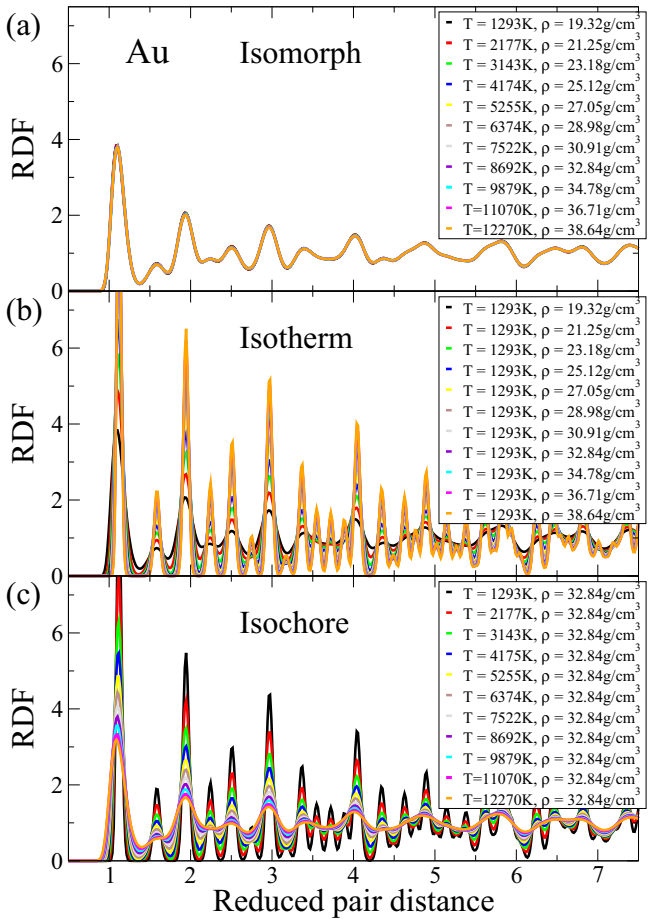

FIG. 4. The radial distribution functions (RDFs) plotted in reduced units [see Eq. (8)] for the case of gold. From top to bottom, the panels show the RDFs for state points that are respectively isomorphic, isothermal, and isochoric to each other. The top panel shows the data collapse along an isomorph as predicted by isomorph theory. Isomorph and isotherm share the state point indicated by the black line, while isochore and isomorph match at the purple line (this is done to avoid melting of the crystal along the isochore; the highest temperature is probably above the melting temperature, however, meaning that this is a superheated state).

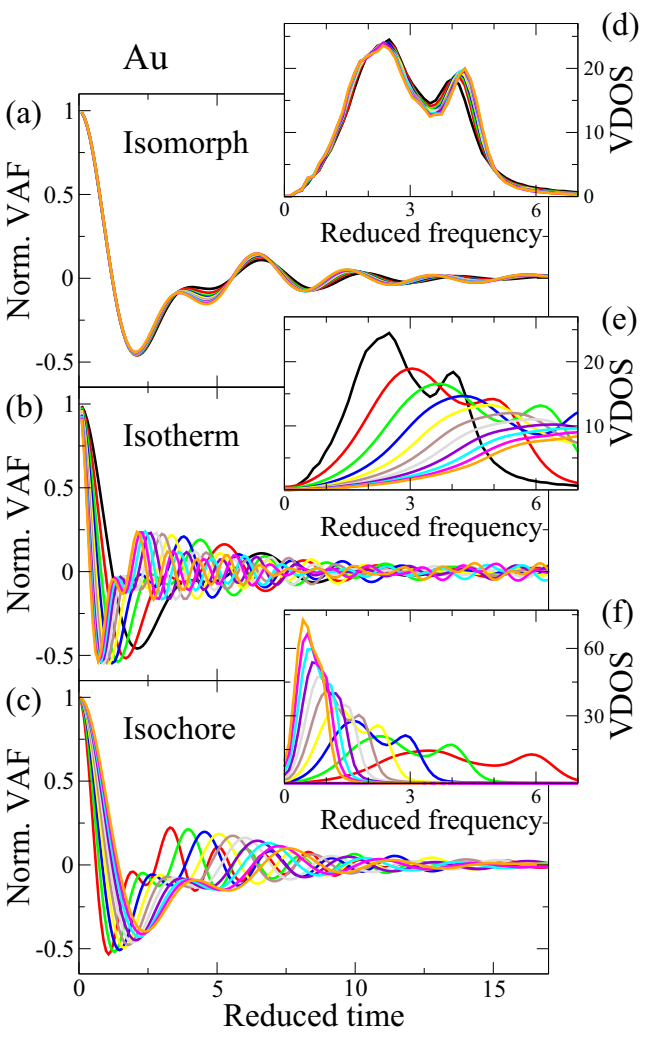

FIG. 5. The figure shows the normalized velocity autocorrelation function (VAF) for the same state points as in Fig. 4. The insets depict the respective phonon or vibrational densities of states (VDOS) obtained from the Fourier transform of the VAF [Eq. (10)]. The predicted data collapse along the isomorph is obeyed, although not as well as in the RDF case.

temperature requires a model that describes both phases with the same accuracy, which is usually not the case [31].

A. Isomorph invariance of structure and dynamics

We start with the results on structure and dynamics. For brevity, the results shown here in detail are from simulations for gold; the other five materials exhibit the same behavior and will be presented in a summarized fashion. A phase diagram is shown in Fig. 3 indicating the isomorph simulated along with the melting curve for the model, to give an idea of where in the phase diagram our focus lies. Some numerical data for gold along the isomorph are shown in Table II. The structure of a system can be quantified by the radial distribution function (RDF), also called pair-correlation function $g(r)$, which is a measure of the probability of finding a particle at a distance r away from a given reference particle. Figure 4 shows the RDF for the reduced pair distance $\tilde{r} = \rho^{1/3} r$ for the state points indicated in the panels, thus along an isomorph, an isotherm, and an isochore, respectively. The peak positions are expected to remain the same also along the isotherm and isochore as a trivial consequence of the reduced pair distance being scaled by $\rho^{1/3}$. Isomorph theory predicts that the structure along an isomorph is invariant, thus we expect all isomorphic RDFs to collapse onto a single curve. Figure 4 validates this to a good approximation, even for large density changes, for the case of gold.

In addition to the structure, also the dynamics of isomorphic state points are predicted to be invariant. The dynamics are studied here by means of the velocity autocorrelation function (VAF). Figure 5 shows the normalized reduced-unit single-particle VAFs obtained from the same simulations and state points of gold as the RDF data. The top, middle, and bottom panels show the VAFs for state points along isomorph, isotherm, and isochore, respectively. The isomorphic curves exhibit a reasonable collapse but with some deviation, especially compared to the near perfect agreement in the RDF

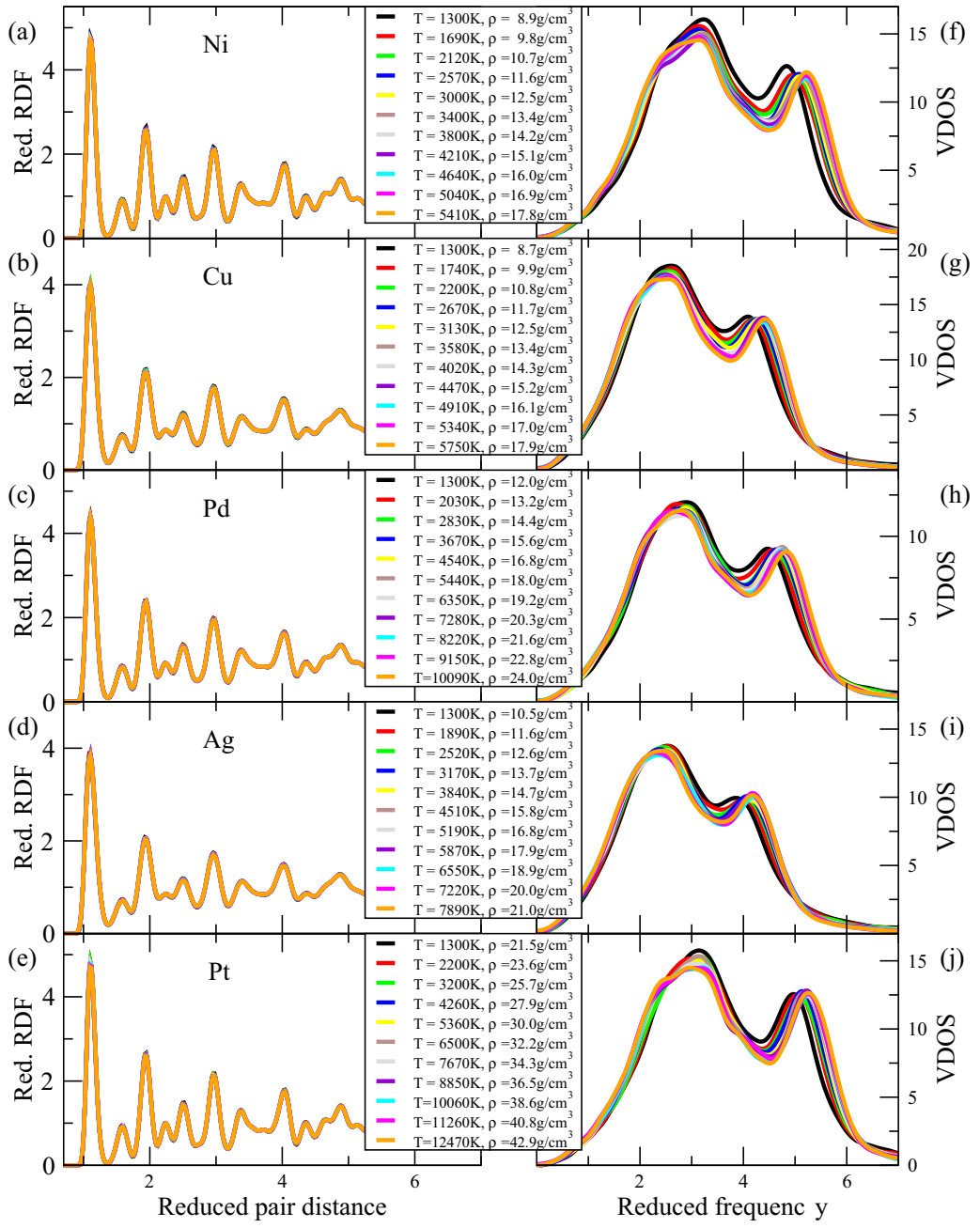

FIG. 6. Radial distribution functions (RDFs) and vibrational densities of states (VDOS) along isomorphs for Ni, Cu, Pd, Ag, Pt. The other five metals confirm the findings for gold, i.e., a near perfect collapse for the structure and a less perfect, but reasonable collapse for the dynamic. The most notable deviations are for the first state point(s).

case. The insets of Fig. 5 show the phonon (vibrational) density of states of their respective curves. The spectrum is related to the Fourier transform of the velocity autocorrelation function via [15]

$$\rho(\omega) = \frac{1}{3NTk_B}\int_{-\infty}^{\infty}\sum_{i=1}^{N}\langle v_i(t)v_i(0)\rangle C(t)\mathrm{e}^{i\omega t}\,dt, \qquad (10)$$

where we include a Gaussian function $C(t) = \exp[-(t/t_c)^2]$ (with t_c chosen to be fixed in reduced units) to smoothly truncate the integrand, which otherwise decays very slowly compared to the data-sampling window.

We obtained similar results for the structure and dynamics of the five other materials simulated, *viz.*, Ni, Cu, Pd, Ag, and Pt; see Fig. 6. Each row shows the RDF on the left and the phonon density on the right, along an isomorph for one metal. All metals demonstrate a comparably good collapse to that found for gold.

B. Other implications of isomorph theory

Another prediction from isomorph theory concerns *isomorph jumps*, which refer to a sudden change in density via a uniform scaling of all particle coordinates and temperature

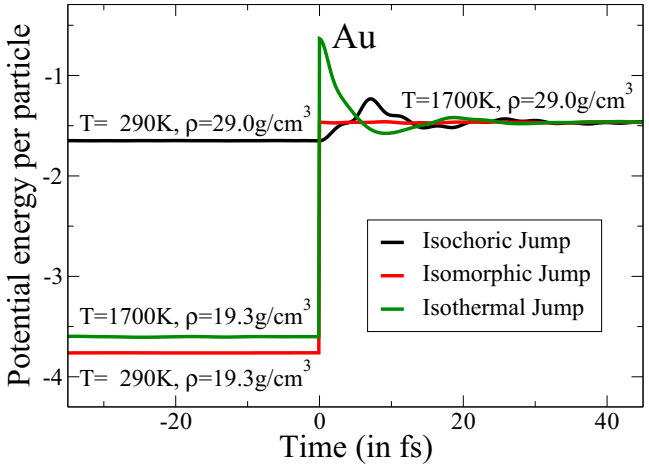

FIG. 7. Potential energy per particle before and after instantaneous jumps at $t = 0$ between the state points indicated. The black and the green lines depict jumps between state points that are, respectively, isochoric and isothermal to each other. Only the red line shows instantaneous equilibration—the line stays flat and does not visibly fluctuate—after the jump.

between state points on the same isomorph. Isomorph theory implies that such a sudden change from a well-equilibrated initial state point should not require further equilibration post jump, predicting the system to be instantaneously in equilibrium at the final state point [3], because the Boltzmann probabilities are unchanged by a jump along an isomorph. This prediction has been validated for viscous liquids, as well as for perfect Lennard-Jones crystals.

The simulations start with runs at the respective starting point to make sure the systems are in equilibrium. At the jump, the density is changed by uniformly scaling all particle coordinates, the temperature for the thermostat is set to the new value, and all velocities are scaled accordingly. The results for gold can be found in Fig. 7, showing the potential energy per particle before ($t < 0$) and after ($t > 0$) jumps to the point indicated in the figure. The initial points have been chosen to be isothermal (green), isochoric (black) and isomorphic (red) to the final state point. The red line validates the prediction as it shows no visible fluctuations in the potential energy post jump. The system is instantaneously in equilibrium as evidenced by the red line staying perfectly flat (apart from normal equilibrium fluctuations, not visible here). In contrast to this, the black and the green lines are clearly not in equilibrium, and the potential energies oscillate towards the new level after the jump.

Since many mechanical properties in crystals are associated with the existence of defects in the lattice and these properties are also expected to be isomorph invariant, we examine this in the following for the case of vacancy diffusion. A vacancy in the lattice is an empty spot from which the atom has been removed. This introduces a new kind of dynamics to the crystal since atoms can now jump to the new, empty positions on the lattice, resulting in the vacancies moving around. Vacancy diffusion is quantified by means of the mean-square displacement (MSD) of the atoms [14,32]. Figure 8 shows the MSD along isomorph, isochore and isotherm for

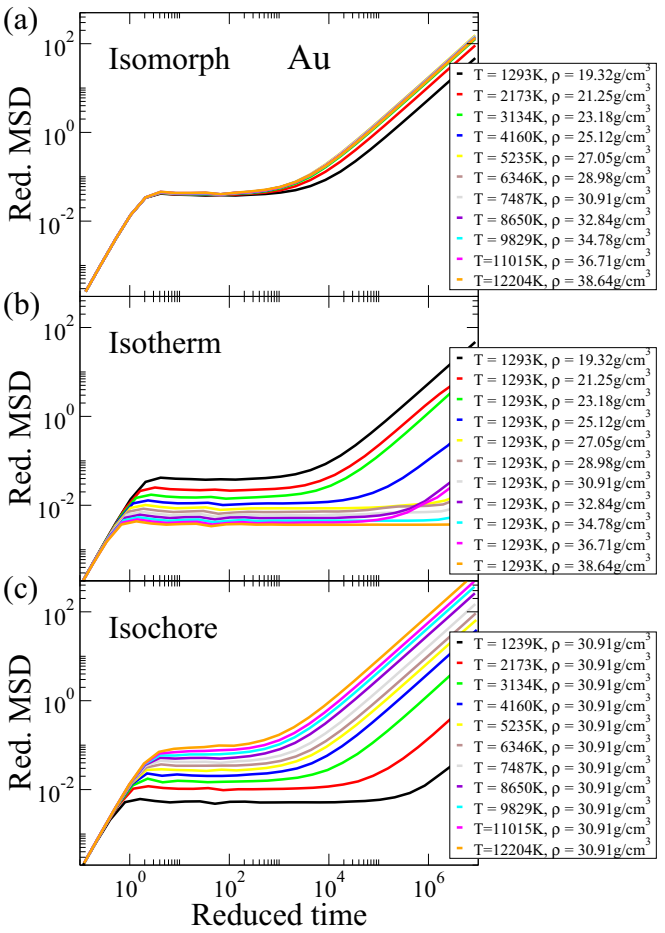

FIG. 8. Mean-squared displacement (MSD) for the state points indicated. To generate vacancies, four randomly selected atoms have been removed from the initial crystal. The collapse exhibited along the isomorph is good in the ballistic regime (trivial) and the plateau (less trivial), while the diffusive part shows some deviations, especially for the lowest density state point. (Note that the isochore has a slightly different density than that of Fig. 4.)

the case of four particles removed from a $10 \times 10 \times 10$ fcc crystal of gold, corresponding to a vacancy concentration of 10^{-3}, which is only slightly higher than the experimental concentration close to melting, 7×10^{-4} [33]. The isomorph used for studying diffusion was redetermined using the DIC, leading to slightly different temperatures.

The figure shows an approximate collapse along the isomorph, although there is a noticeable deviation for the first two curves (the lowest two densities). The collapse is poorer than that seen for the Lennard-Jones crystal in Ref. [14]. This can be partly explained by observing that the starting state point in the present case is closer (in density) to the triple point than was the case for the Lennard-Jones results, although the pressure in our simulations is still large by experimental standards (see Table II). The prediffusive parts of the curves collapse well. For the initial ballistic regime the MSD is proportional to time squared, which is a trivial consequence of the use of reduced units and has nothing to do with isomorph invariance (this is seen also for the isochore and isotherm). But the invariance of the height and

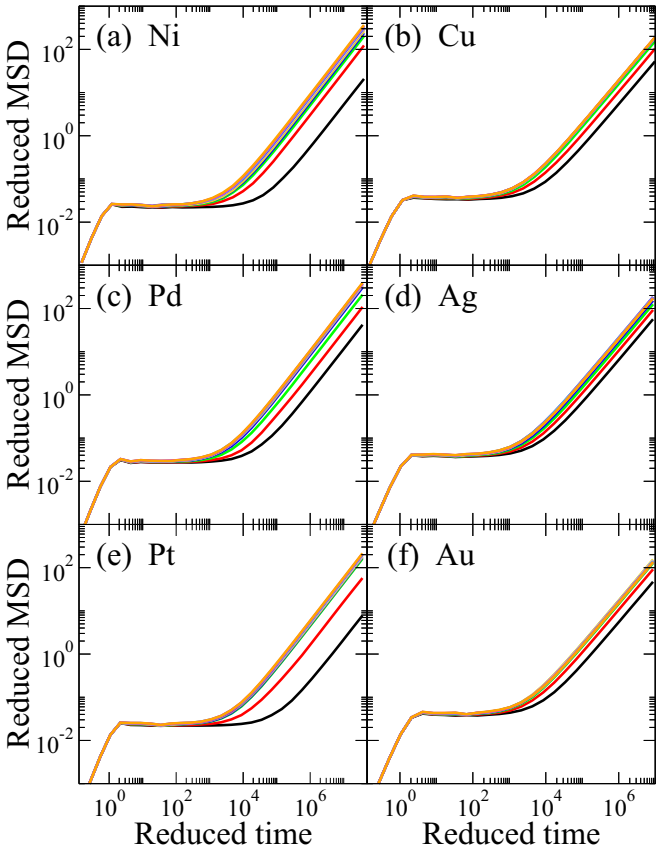

FIG. 9. Mean-squared displacement along isomorphs for the six metals with four vacancies (the bottom right panel depicting gold shows the same data as the top panel of Fig. 8).

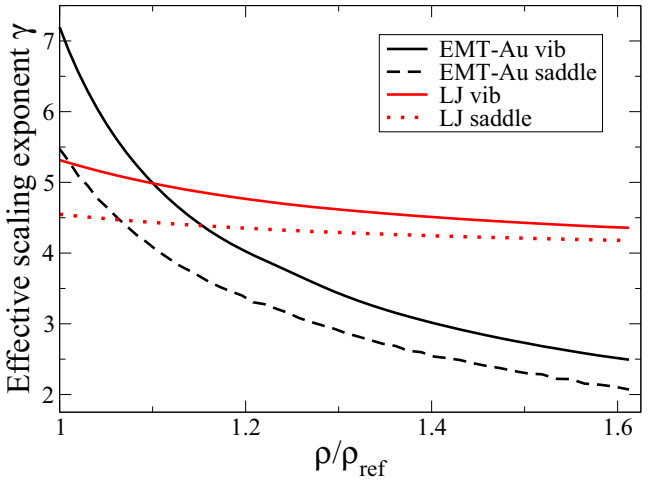

FIG. 10. Effective scaling exponent for specific configurations determined using EMT potential for gold and the Lennard-Jones (LJ) potential. The vibrational configurations, one for each system, were sampled from an NVT run of the perfect crystal at density $\rho_{\text{ref}} = 19.3$ g/cm^3 and temperature 1300 K for Au, density $\rho_{\text{ref}} = 1.05\sigma^{-3}$, and temperature 0.630 ϵ/k_B for LJ. The potential energy relative to the perfect lattice was determined for a range of densities (scaling both the perfect lattice and the vibrational configuration). The saddle configurations are the unrelaxed saddle point between vacancy hopping, constructed by moving a neighbor atom of the vacancy in an otherwise perfect crystal halfway towards the vacant site. The energy difference between the unrelaxed saddle point and the unrelaxed vacancy was determined for the same range of densities. The effective scaling exponents given by the logarithmic derivatives $d\ln U/d\ln\rho$ are plotted against the reduced densities ρ/ρ_{ref}.

the location of the onset of the plateau are nontrivial aspects of the vibrational dynamics. The diffusivity (corresponding in the double-logarithmic representation to the height of the long-time part of the MSD curves) is presumably determined by a single energy barrier associated with vacancy hopping. The poor collapse of the curves here therefore implies that this energy barrier scales in a slightly different manner than the potential energy surface near the ground state—it is the latter which controls vibrational dynamics whose fluctuations determine the isomorph.

Figure 9 shows the MSD along an isomorph in all six fcc metals with each crystal having four vacancies. The bottom right panel shows the same gold isomorph as in the previous figure. The same overall behavior is observed in the other metals, i.e., that the higher density and temperature points collapse well while the first (two) curve(s) exhibit an outlier behavior. This is more notable for the materials on the left-hand side; these have incomplete d-shells, corresponding to stronger bonding and higher melting points, therefore the simulated isomorphs (which all start at the same temperature) are further below the melting line in these cases.

Results for a single vacancy and 16 vacancies in the same $10 \times 10 \times 10$ fcc crystal of the six metals can be found in Appendix B. Both cases exhibit a much worse collapse than the case of four vacancies. For 16 vacancies, visualization (snapshot included in Appendix B) shows that the vacancy concentration is too high, which causes them to cluster together early on in the simulation runs. We thus in this case inadvertently probed void migration rather than vacancy diffusion. Especially interesting is the case of one vacancy where clustering is not an issue. We found a failure to collapse much like Albrechtsen and Olsen found for Lennard-Jones crystals with only one vacancy [34]. This case seems especially sensitive to departures from isomorph invariance (see also the discussion of Fig. 10), but at present we do not have a good explanation of this deviation.

IV. DISCUSSION

The overall results presented here are consistent with expectations from the work of Hummel *et al.*, which showed that most metals in the liquid state have a high virial potential-energy correlation coefficient R [Eq. (1)] and are therefore R-simple. As such they are expected to have good isomorphs. The present work has concentrated on the crystal phase at moderate and high temperatures to avoid quantum effects. The analysis is similar to that undertaken by Albrechtsen *et al.* for Lennard-Jones and other simple model systems including simple molecules [14].

The basic predictions of isomorph theory are invariance of structure and dynamics when the observables are expressed in reduced units: lengths in terms of the interparticle spacing $\rho^{-1/3}$, energies in terms of the temperature k_BT, and times in

terms of the time a particle with the thermal velocity would take to move an interparticle spacing [Eq. (8)]. With these units we find an excellent collapse of the radial distribution function. For the dynamics of the perfect crystal we studied the velocity autocorrelation function (VAF) and its Fourier transform, which can be interpreted as an effective vibrational density of states (VDOS). Here we observed an approximate collapse, clearly worse than the RDF, and also worse than the collapse seen for the Lennard-Jones crystal in Ref. [14]. We validated the prediction of instantaneous equilibration for isomorph jumps. To study dynamics beyond vibrations we simulated a system with vacancies and monitored the mean squared displacement. The collapse here was also approximate, in fact poorer than for the VAF, suggesting that the relevant energies (around the saddle point of the vacancy hopping process) scale somewhat differently with density than energies near ground state (perfect crystal), which are relevant for vibrations. In particular one can imagine that the local density experienced by the hopping atom at the top of the energy barrier is quite different from the densities of the surrounding atoms, corresponding to different effective γ.

The combination of locally high density at the saddle point for the hopping atom and the strong density dependence of the density-scaling exponent for EMT systems suggests a scenario like this. As a crude test we consider the energy of the "unrelaxed saddle point" relative to that of the unrelaxed vacancy, as well as the energy of a typical vibrational configuration of the defect-free lattice, drawn from a simulation at a specific temperature, relative to that of the perfect lattice. The unrelaxed vacancy is the perfect lattice with one atom removed. The unrelaxed saddle point is the configuration obtained by displacing a neighbor of the removed atom exactly halfway towards the empty site. The logarithmic derivatives of these energy differences give a kind of "configuration-specific" density-scaling exponent γ, plotted in Fig. 10. There is a significant reduction in the effective scaling exponent for the unrelaxed saddle-point energy compared to that of the vibrational energy (5.5 versus 7.2 at the initial density). Since vibrational fluctuations dominate the determination of the γ used to generate isomorphs, the lower scaling exponent for saddle points means these configurations have a lower energy than expected as one moves along the isomorph, which is why the diffusivity in reduced units is higher than than for the reference state point. The contrast between the energy fluctuations used to determine the isomorph and those relevant for the dynamics is greater for a defective crystal than for a liquid or amorphous solid, allowing such deviations from perfect isomorph scaling to arise. The figure includes also results of the same calculation for the Lennard-Jones crystal, where there is also a difference, albeit smaller than in the EMT case. The presence of this difference is consistent with the lack of collapse for a single vacancy noted in Ref. [34], while its small size explains the generally better collapse found in Ref. [14]. It remains unclear why including several vacancies then gives a better collapse; it presumably involves the interactions between them (including vacancy binding and unbinding) reducing the contrast between the energy fluctuations used to determine the isomorph and the relevant saddle-point energy which governs vacancy dynamics. In a sense it is not that surprising that the specific parts of the potential

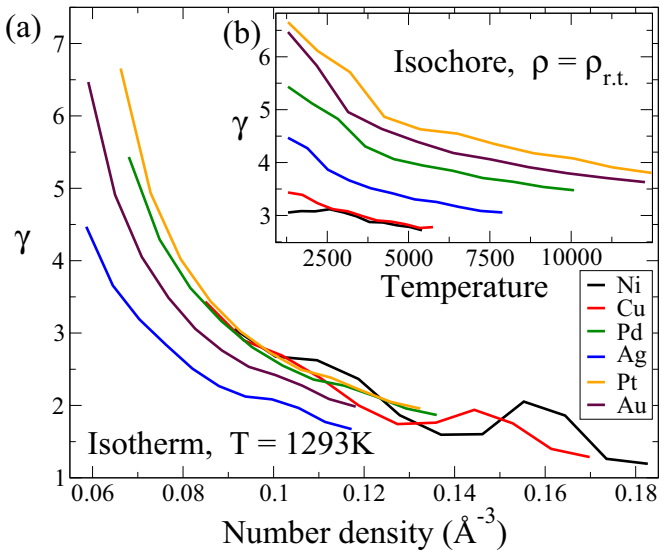

FIG. 11. Variation of γ for the six fcc metals along the $T = 1293$ K isotherm in the main panel (a). The inset (b) shows the same variation along isochores where $\rho = \rho_{r.t.}$ is the respective room temperature density of the metal. The γ variations are clearly dominated by changes in density. The bumps visible in the low γ regime, most notable in the Cu and Ni isotherms, are due to the cutoff as detailed in Appendix C.

energy function associated with vacancy hopping behave differently under density changes compared to those related to vibrations. Thus, while less pronounced in the Lennard-Jones case, the same deviations occur in both systems. This kind of nonuniform scaling could possibly also be the root of the failure to get a good collapse of the VAF, although in that case we do not see quite the same "outlier" behavior for the low density (temperature) data, except perhaps for Ni.

The general degree of isomorph invariance is similar for the different metals (see Fig. 6 for the radial distribution functions and phonon density of states, and Fig. 9 for the vacancy diffusion), which is not surprising since the same functional form of interatomic interactions is used for all of them. In the future, it is important to investigate isomorph invariance of these metals using other types of potentials, for example, EAM.

Unlike in other systems, the density-scaling exponent γ is strongly state point dependent when using the EMT potential. The main panel in Fig. 11 shows the variation of γ for the six fcc metals with changing density at constant temperature. The behavior for increasing temperature at fixed density can be seen in the inset. It is evident that the change in γ is dominated by changing density and only mildly decreasing with temperature. Thus, the variation of γ along an isomorph (not pictured) displays a similar behavior to that of the isotherms. The oscillatory behavior along the isotherms in the low γ region, most obvious in the cases of Ni and Cu, is an artifact due the cutoff and occurs when increasing the density pushes a new neighbor shell through the cutoff distance (see Appendix C).

Next we discuss briefly the connection between the density-scaling exponent γ, of the two most important parameters (together with R) in isomorph theory and the Grüneisen

TABLE III. Comparison of experimental Grüneisen parameters with EMT values at ambient pressure and temperature.

Sym.	γ_G (exp.)	γ_G (EMT)
Ni	1.88[(a)]	1.9
Cu	1.96[(a)]	2.1
	1.99[(b)]	
Pd	2.33[(c)]	3.4
Ag	2.40[(a)]	2.8
	2.33[(b)]	
Au	2.94[(b)]	4.2
Pt	2.54[(a)]	4.3

[(a)]Ref. [35].
[(b)]Ref. [36].
[(c)]Ref. [37].

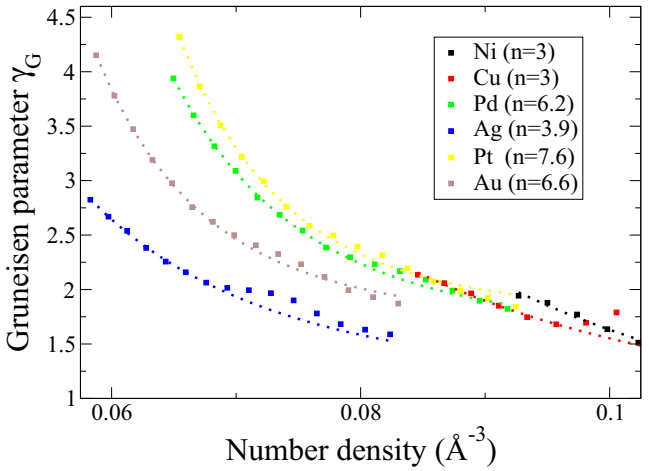

FIG. 12. Gruneisen parameter γ_G for the six metals as a function of (number) density at temperature 300 K (squares). The dotted lines show fits to the functional form $a + b/\rho^n$, with the exponent n indicated for each metal in the legend. The data show small bumps associated with the cutoff artifact mentioned above for the fitting only the data at small densities were used. For Cu and Ni allowing the exponent to vary leads to negative values of the additive constant a and here the exponent was fixed at $n = 3$.

parameter γ_G, which is an important thermodynamic parameter in the study of solids. The latter plays a fundamental role in the Mie-Grüneisen equation of state, often used to model metals at high pressures. Pandya *et al.* [38] argue that the Grüneisen parameter, involving as it does third derivatives of the potential, is a stringent test of a model of a solid. Reference [39] discusses the use of a pressure-dependent Grüneisen parameter to estimate the melting curves of silver, gold, and copper at high pressure. Insight from isomorph theory and the study of the isomorphic properties of metals can help to understand the density dependence of γ and by extension γ_G. The microscopic definition of γ_G involves the density dependence of normal mode frequencies, but we focus on the macroscopic or thermodynamic definition

$$\gamma_G \equiv V \frac{\alpha_p K_T}{C_V} \tag{11}$$

where α_P is the thermal expansion coefficient, K_T the isothermal bulk modulus, and C_V the isochoric specific heat. The relation

$$\gamma_G = \frac{\gamma C_V^{\mathrm{ex}} + N k_B}{C_V} \tag{12}$$

between γ and γ_G—where C_V^{ex} is the excess part of the isochoric heat capacity C_V—was derived in Ref. [18] and is exact within the classical approximation. Typically γ is greater than γ_G by around a factor of two. Using Eq. (12), Hummel *et al.* compared values of γ determined from the experimental values of γ_G for liquid metals to values determined from their DFT calculations (see their Fig. 5). In Table III we compare values of γ_G determine for the crystal phase at ambient temperature and pressure to values determined for EMT. We find good agreement for Cu and Ni, while the other values are significantly overestimated compared to experiment. From Table I for the comparison of γ between EMT and DFT for the liquid, and from the work of Hummel *et al.* who compared DFT results for γ with values inferred from experimental Gruneisen parameters, we can infer that for Au and Ag the EMT values match the DFT values reasonably well, but both overestimate the experimental values of γ and γ_G. For Pd and Pt the DFT results match experiment, but the EMT results are too high.

There is interest in the literature in the density dependence of γ_G, for example, for understanding the state of matter deep in the earth's interior [36,38]. A frequently used empirical model for the density dependence is $\gamma_G \rho = \text{const}$, i.e., the Grüneisen parameter decreases inversely with density. This is consistent with our observation that γ is mainly a function of density and for EMT metals decreases strongly with density; however, our data do not support a $1/\rho$ dependence of γ_G (see Fig. 12). A closer look at the functional form of the EMT potential should provide some clues for the density dependence of both γ and γ_G.

Finally we discuss implications for the thermodynamics of melting and freezing of metals. An early prediction of the isomorph theory was that the melting curve follows an isomorph for R-simple systems [3]. This follows from the general idea that the structure is invariant. Considering constant volume conditions in the coexistence region, ensuring the presence of a fixed amount of each phase, a broad interpretation of "structure" would include "degree of crystallization," and would have the consequence that the melting curve must follow an isomorph (otherwise the degree of crystallization along an isomorph would vary). However, for realistic systems isomorph invariance applies to a single phase, but not a system containing two phases with different densities. In the latter case terms in the free energy which depend on density only become relevant, affecting the position of the melting curve while having no relevance for the structure and dynamics of a single phase. This has been studied in detail in Refs. [40] and [41]. In particular the theory developed in Ref. [40] allows calculation of the freezing and melting lines using isomorphs as the basis for a perturbative approach. Computer simulations confirmed the predictions for the Lennard-Jones case. The data in Fig. 3 for the melting curve seem not to coincide with crystal isomorph, though data for the freezing line for

the same system (not shown) coincide very closely with a liquid isomorph. The methods of Ref. [40] should allow both to be calculated from simulations at a single temperature. Applied to more computationally demanding first-principles methods, such as DFT, this gives the possibility to make accurate melting curve determinations at high pressures.

In summary, we have shown that isomorph theory applies well to fcc metals simulated using the effective medium theory many-body potential. We find the expected invariance of structure and, slightly less perfectly, of vibrational dynamics. Instantaneous equilibration following an isomorph jump is also seen. Slightly larger deviations emerge when studying defect dynamics. This was argued to be a consequence of, on one hand, the contrast between the configurations governing (in this case) vacancy hopping and those dominating the fluctuations, and on the other hand, the strong density dependence of γ.

ACKNOWLEDGMENTS

We thank the anonymous reviewer who suggested the self-consistency check for the direct isomorph check and the analytical fit used in Fig. 12. The work was supported by the VILLUM Foundation's *Matter* Grant (No. 16515).

APPENDIX A: VALIDATION OF THE DIRECT ISOMORPH CHECK

We present two different ways of validating the direct isomorph check. The first is to compare with an isomorph generated by numerical integration of Eq. (7) using density steps of 1%. This is an accurate method for generating isomorphs [3], but is computationally demanding if large density changes are considered. The second validation method requires no extra simulation; instead it checks for self-consistency of the DIC isomorph: After generating the isomorph and simulating those state points, the actual γ values can be plotted as a function of density and fitted to a simple function $\gamma(\rho) = a + b/\rho^n$. An example of such a fit is shown in the inset of Fig. 13. Integration of this yields the form $\ln T = \ln T_0 + a \ln \rho/\rho_0 + b(1/\rho^n - 1/\rho_0^n)/n$ for some starting point ρ_0, T_0. Both this and the numerical step-by-step generation of the isomorph are shown in Fig. 13. The stepwise-generated isomorph has a temperature within 0.5% of the DIC isomorph at the highest density. The analytic integration based on the fitting procedure underestimates it by about 2%, probably due to the small deviations between of the fit from $\gamma(\rho)$ visible in the inset. Had the stepwise isomorph not been available, this could be considered a reasonable validation of the DIC.

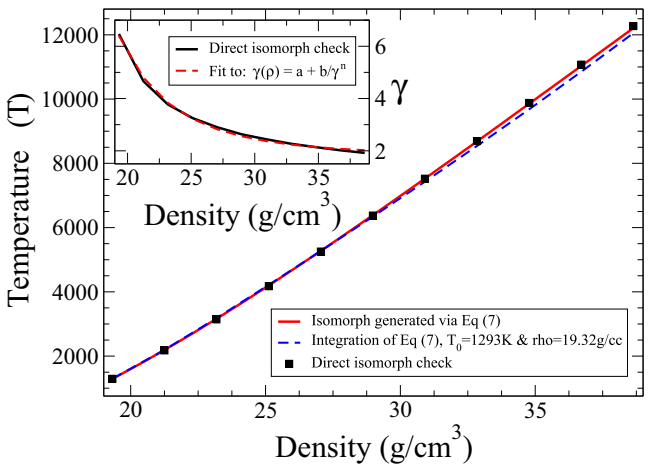

FIG. 13. Comparison between the isomorphic state points generated from the direct isomorph check and integration of Eq. (7) for Au. The inset shows a fit of $\gamma(\rho) = a + b/\rho^n$ with parameters $a = 1.823$, $b = 2.977 \times 10^6$, $n = 4.520$; analytic integration of Eq. (7) using this functional form starting from the lowest density yields the dashed curve. Numerical integration of Eq. (7) from the lowest density using the γ values determined along the way yields the smooth red curve.

APPENDIX B: TESTING DIFFERENT NUMBERS OF VACANCIES

The failure of the diffusive part of the mean-squared displacement to collapse along an isomorph is shown in Fig. 14 for the case of one vacancy and in Fig. 15 for 16 vacancies. Reasons that spoil isomorph invariance in the respective cases are discussed in the main text. Figure 16 shows a snapshot of the clustered vacancies in the 16 vacancies case; here the larger, pink spheres indicate the empty lattice positions while the actual particles were removed for better visibility,

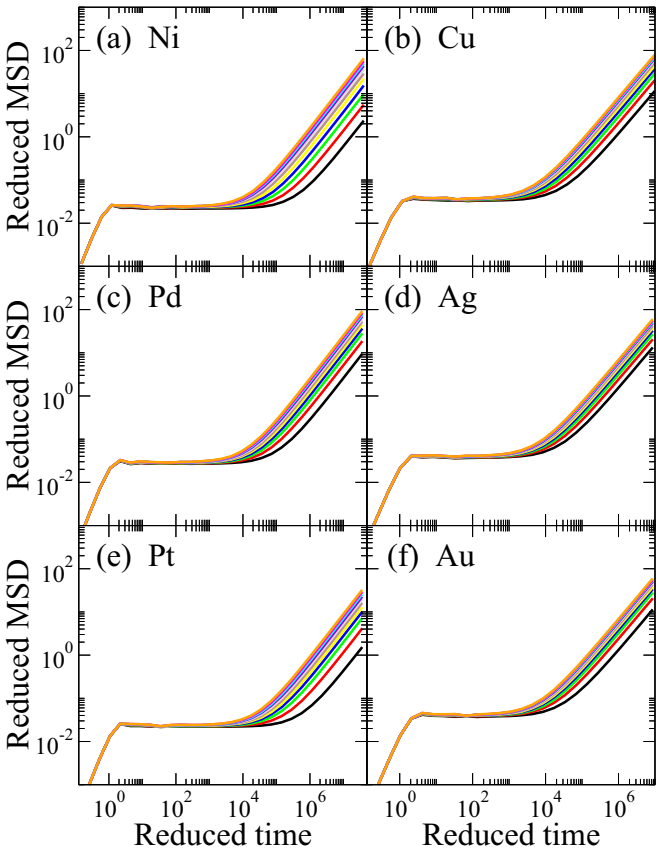

FIG. 14. MSD along isomorphs after removing one out of 4000 particles.

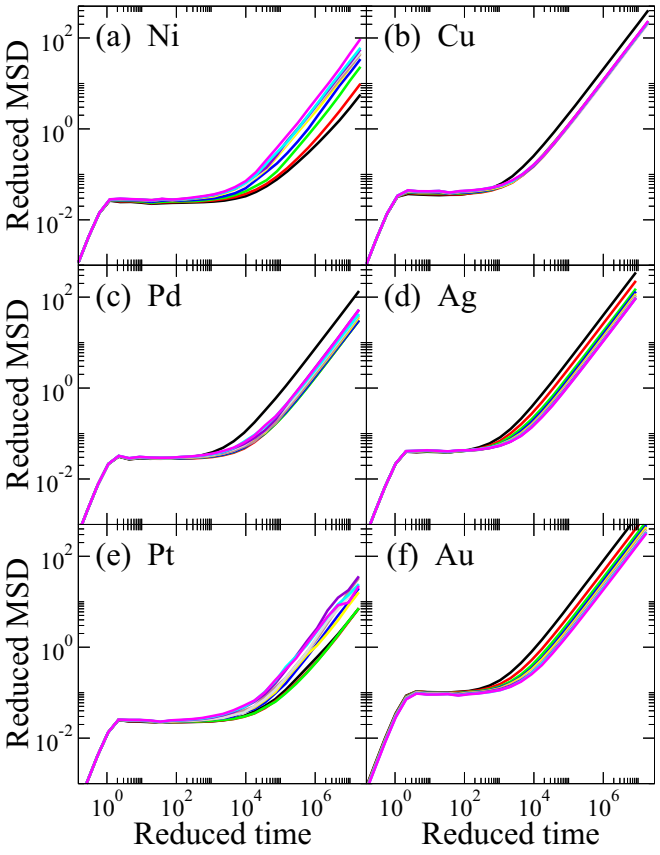

FIG. 15. MSD along isomorphs after removing 16 out of 4000 particles.

while the gray spheres are a guide to the eye and indicate the corners of the simulation box. The movie obtained from several of these "inverted" configurations shows that these kind of clusters form early on in the simulation and do not disperse again.

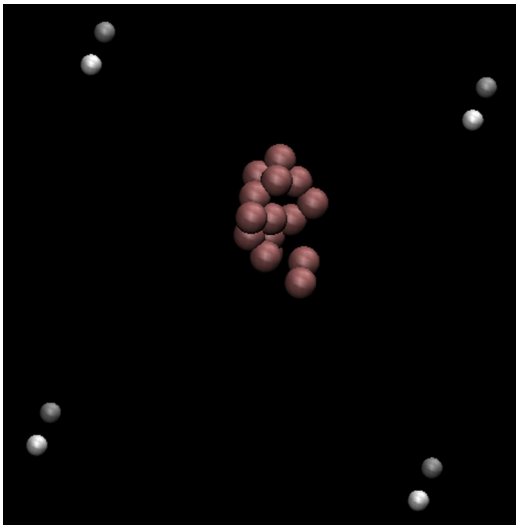

FIG. 16. Snapshot of the clustering of 16 vacancies in gold. The picture shows a "negative" of the simulation. The pink spheres indicate the vacant lattice points, and the actual particles have been removed. The gray spheres indicate the corners of the simulation box.

APPENDIX C: CUTOFF ARTIFACT

An explanation is given here as to how the bumplike artifacts in the density dependence of γ for Cu and Ni (Fig. 11) arise. They occur when successive neighbor shells pass through the cutoff. The latter is implemented in the form of a smoothed step function (a Fermi function) modulating the interactions: Noting that the distance to the nth shell of the zero-pressure, zero-temperature fcc lattice, d_n, is given by $d_n = \sqrt{n}d_1$, where $d_1 = \frac{a}{\sqrt{2}}$ is the nearest neighbor distance, then the half-way point of the Fermi function is set to lie between the neighboring shells n and $n+1$ at

$$r_c = d_1 \frac{(\sqrt{n} + \sqrt{n+1})}{2} \tag{C1}$$

with the default choice $n = 3$. The fcc lattice constant a can be expressed in terms of the number density ρ as follows:

$$\rho a^3 = 4 \;\Leftrightarrow\; a = (4/\rho)^{1/3}. \tag{C2}$$

This yields the distance to the nth shell in terms of the density:

$$d_n = \sqrt{n}d_1 = \sqrt{n}\frac{a}{\sqrt{2}} = \sqrt{\frac{n}{2}}\left(\frac{4}{\rho}\right)^{1/3}. \tag{C3}$$

The densities at which the $n > 3$ shells pass through the middle of the cutoff, can be found through equating Eqs. (C3) and (C1) setting $n = 3$ in the latter:

$$\sqrt{\frac{n}{2}}\left(\frac{4}{\rho}\right)^{1/3} = d_1 \frac{(\sqrt{3} + \sqrt{4})}{2}, \tag{C4}$$

$$\rho = 4\left(\frac{\sqrt{2}}{d_1}\frac{\sqrt{n}}{\sqrt{3}+\sqrt{4}}\right)^3. \tag{C5}$$

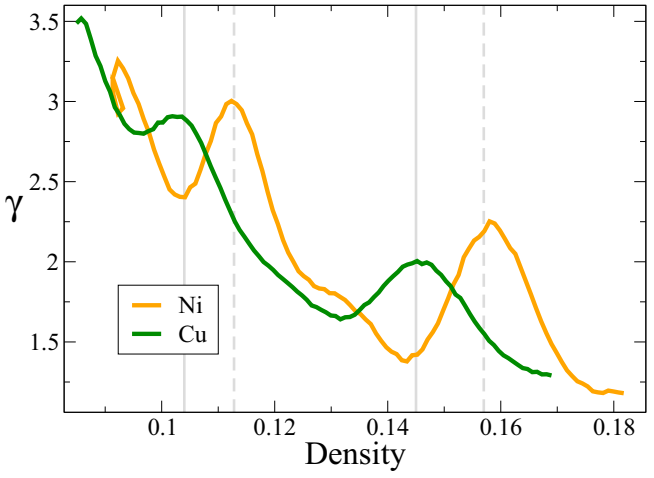

FIG. 17. Oscillatory behavior of density dependence of γ for Cu and Ni due to the cutoff. The light gray lines (solid for Cu, dashed for Ni) indicate the densities at which the radius of the fourth and fifth shells is exactly in the middle of passing through the cutoff.

Insertion of the material dependent nearest-neighbor distances: $d_1^{Ni} = 2.49$ Å, $d_1^{Cu} = 2.56$ Å from the EMT parameters in Ref. [12] yields the following densities:

$$\text{Ni:} \quad \rho_{n=4} = 0.113\,\text{Å}^{-3}, \quad \rho_{n=5} = 0.158\,\text{Å}^{-3} \tag{C6}$$

$$\text{Cu:} \quad \rho_{n=4} = 0.104\,\text{Å}^{-3}, \quad \rho_{n=5} = 0.145\,\text{Å}^{-3} \tag{C7}$$

These densities are marked by light gray lines (solid for Cu and dashed for Ni) in Fig. 17 and coincide with the bumps in the variation of γ. The reason this effect is most visible for these metals is that γ reaches quite small values, which implies (interpreting γ as arising from an effective inverse power law exponent) a relatively long-ranged effective interaction and that contributions from distant neighbors are more significant than is the case for higher values of γ.

[1] N. W. Ashcroft and N. D. Mermin, *Solid State Physics* (Saunders College, Orlando, Florida, 1976).
[2] G. Gottstein, *Physical Foundations of Materials Science* (Springer, Heidelberg, Germany, 2004).
[3] N. Gnan, T. B. Schrøder, U. R. Pedersen, N. P. Bailey, and J. C. Dyre, J. Chem. Phys. **131**, 234504 (2009).
[4] F. Hummel, G. Kresse, J. C. Dyre, and U. R. Pedersen, Phys. Rev. B **92**, 174116 (2015).
[5] A. L. Jensen, C. Køneke, C. Kjeldbjerg, F. S. Mahler, J. Olsen, and M. Bennetsen, Påvisning af isomorfer i metalliske væsker, Bachelor's thesis, Roskilde University, 2017.
[6] N. P. Bailey, U. R. Pedersen, N. Gnan, T. B. Schrøder, and J. C. Dyre, J. Chem. Phys. **129**, 184507 (2008).
[7] Y.-C. Hu, B.-S. Shang, P.-F. Guan, Y. Yang, H.-Y. Bai, and W.-H. Wang, J. Chem. Phys. **145**, 104503 (2016).
[8] D. C. Wallace, *Thermodynamics of Crystals* (Courier Corporation, Mineola, New York, 1998), pp. 104–105.
[9] H. C. Andersen, J. D. Weeks, and D. Chandler, Phys. Rev. A **4**, 1597 (1971).
[10] C. M. Roland, S. Bair, and R. Casalini, J. Chem. Phys. **125**, 124508 (2006).
[11] T. S. Ingebrigtsen, L. Bøhling, T. B. Schrøder, and J. C. Dyre, J. Chem. Phys. **136**, 061102 (2012).
[12] K. W. Jacobsen, P. Stoltze, and J. K. Nørskov, Surf. Sci. **366**, 394 (1996).
[13] N. P. Bailey, T. S. Ingebrigtsen, J. S. Hansen, A. A. Veldhorst, L. Bøhling, C. A. Lemarchand, A. E. Olsen, A. K. Bacher, L. Costigliola, U. R. Pedersen, H. Larsen, J. C. Dyre, and T. B. Schrøder, SciPost Phys. **3**, 038 (2017).
[14] D. E. Albrechtsen, A. E. Olsen, U. R. Pedersen, T. B. Schrøder, and J. C. Dyre, Phys. Rev. B **90**, 094106 (2014).
[15] C. Lee, D. Vanderbilt, K. Laasonen, R. Car, and M. Parrinello, Phys. Rev. B **47**, 4863 (1993).
[16] A. Kelly and K. M. Knowles, *Crystallography and Crystal Defects* (John Wiley & Sons, Chichester, West Sussex, 2012).
[17] N. P. Bailey, U. R. Pedersen, N. Gnan, T. B. Schrøder, and J. C. Dyre, J. Chem. Phys. **129**, 184508 (2008).
[18] T. B. Schrøder, N. P. Bailey, U. R. Pedersen, N. Gnan, and J. C. Dyre, J. Chem. Phys. **131**, 234503 (2009).
[19] T. B. Schrøder, N. Gnan, U. R. Pedersen, N. P. Bailey, and J. C. Dyre, J. Chem. Phys. **134**, 164505 (2011).
[20] T. B. Schrøder and J. C. Dyre, J. Chem. Phys. **141**, 204502 (2014).
[21] A. Tölle, H. Schober, J. Wuttke, O. G. Randl, and F. Fujara, Phys. Rev. Lett. **80**, 2374 (1998).
[22] A. Tölle, Rep. Prog. Phys. **64**, 1473 (2001).
[23] R. Casalini and C. M. Roland, Phys. Rev. E **69**, 062501 (2004).
[24] G. Tarjus, D. Kivelson, S. Mossa, and C. Alba-Simionesco, J. Chem. Phys. **120**, 6135 (2004).
[25] C. Alba-Simionesco, A. Cailliaux, A. Alegria, and G. Tarjus, Europhys. Lett. **68**, 58 (2004).
[26] R. Casalini, U. Mohanty, and C. M. Roland, J. Chem. Phys **125**, 014505 (2006).
[27] RUMD software is freely available at http://rumd.org.
[28] W. Haynes, *CRC Handbook of Chemistry and Physics*, 95th ed. (CRC Press, Boca Raton, Florida, 2014).
[29] U. R. Pedersen, J. Chem. Phys. **139**, 104102 (2013).
[30] P. W. Mirwald and G. C. Kennedy, J. Geophys. Res. **84**, 6750 (1979).
[31] D. Alfe, L. Vočadlo, G. Price, and M. Gillan, J. Phys.: Condens. Matter **16**, S973 (2004).
[32] J. Vaari, Solid State Ion. **270**, 10 (2015).
[33] R. O. Simmons and R. W. Balluffi, Phys. Rev. **125**, 862 (1962).
[34] D. E. Albrechtsen and A. E. Olsen, Undersøgelser af isomorfer i krystaller, Master's thesis, Roskilde University, 2013.
[35] C. Kittel, *Introduction to Solid State Physics*, 2nd ed. (Wiley, New York, 1956).
[36] F. Quareni and F. Mulargia, Phys. Earth Planet. Inter. **55**, 221 (1989).
[37] T. F. Smith and G. K. White, J. Phys. F **7**, 1029 (1977).
[38] C. Pandya, P. Vyas, T. Pandya, and V. Gohel, Bull. Mat. Sci. **25**, 63 (2002).
[39] H. K. Hieu and N. N. Ha, AIP Adv. **3**, 112125 (2013).
[40] U. R. Pedersen, L. Costigliola, N. P. Bailey, T. B. Schrøder, and J. C. Dyre, Nat. Commun. **7**, 12386 (2016).
[41] U. R. Pedersen, K. Adrjanowicz, K. Niss, and N. P. Bailey, SciPost Phys. **2**, 022 (2017).